An enhancement to sea ice motion and age products at NSIDC

Mark A. Tschudi[1], Walter N. Meier[2], J. Scott Stewart[2]

[1]CCAR, Department of Aerospace Engineering Sciences, University of Colorado-Boulder, UCB 431, Boulder, CO, USA, 80309

[2]National Snow and Ice Data Center, CIRES, University of Colorado-Boulder, UCB 449, Boulder, CO, USA, 80309

Correspondence to: Mark A. Tschudi (mark.tschudi@colorado.edu)

Abstract. A new version of sea ice motion and age products includes several significant upgrades in processing, corrects known issues with the previous version, and updates the time series through 2018, with regular updates planned for the future. First, we provide a history of these NASA products distributed at the National Snow and Ice Data Center. Then we discuss the improvements to the algorithms, provide validation results for the new (Version 4) and older versions and intercompare the two. While Version 4 algorithm changes were significant, the impact on the products is relatively minor, particularly for more recent years. The changes in Version 4 reduce motion biases by ~0.01 to 0.02 cm/s and error standard deviations by ~0.3 cm/s. Overall ice speed increased in Version 4 over Version 3 by 0.5 to 1.0 cm/s over most of the time series. Version 4 shows a higher increasing trend of 0.21 cm/s/decade compared to 0.13 cm/s/decade for Version 3. The new version of ice age estimates indicates more older ice than Version 3, especially earlier in the record, but similar trends toward less multi-year ice. Changes in sea ice motion and age derived from the product show a significant shift in the Arctic ice cover, from a pack with a high concentration of older ice, to a sea ice cover dominated by first-year ice, which is more susceptible to summer melt. We also observe an increase in the speed of the ice over the 30+ year time series, which has been shown in other studies and is anticipated with the annual decrease in sea ice extent.

1 Introduction

Arctic sea ice conditions have undergone significant changes in recent years with dramatic reductions in the overall ice extent, ice age, and ice thickness. The decline in Arctic sea ice extent is one of the better-known and more striking examples of a changing Arctic [e.g. *Meier et al.*, 2014; *Comiso et al.*, 2008;

2012; 2017a; *Stroeve et al.*, 2011; 2014]. Recent estimates indicate that September Arctic sea ice extent has decreased by approximately 13% per decade since 1979, with record or near-record minimum extents occurring several times in the last few years [e.g., *Perovich et al.*, 2018]. In the Antarctic, the trends are smaller and there is higher interannual variability [e.g., *Parkinson and Cavalieri*, 2012]; overall the Antarctic trends are slightly positive, but with strong regional variability [*Comiso et al.*, 2017b].

Data on sea ice thickness are far less comprehensive and it is more difficult to determine solid quantitative thickness or volume trends. However, there is broad evidence, from observations [e.g., *Kwok*, 2018] and models [e.g., *Stroeve et al.,* 2014] that Arctic sea ice thinning trends are even stronger than the extent decrease. One explanation for the stronger decline in ice thickness is the preferential loss of thicker, old ice in comparison with relatively thin first-year ice. For example, *Johannessen et al.* [1999] and *Comiso et al.* [2008, 2012] noted the decline in multiyear sea-ice was roughly twice that of first-year ice. In a study examining ice age since the early 1980s, *Maslanik et al.* [2011] found continued recent loss of the oldest ice types, which accelerated starting in 2005. This trend has continued through 2018 [*Perovich et al.*, 2018; *Kwok*, 2018].

A continued decline in the sea-ice cover and the shift from thick multiyear ice (MYI) to more easily navigable first-year ice (FYI) arguably will have one of the biggest impacts on humans and the Arctic environment [e.g., *Pizzolato et al.*, 2016]. In particular, the prospect of new shipping lanes, extraction of oil and gas from previously inaccessible regions, and increased national security concerns associated with easier and more accessible Arctic waters have already been identified as significant economic and cultural changes related to the sea-ice cover [*Huntington et al.*, 2007]. More open water along the coast will also add to the risk of storm surge and coastal erosion [*Vermaire et al.*, 2013; *Francis et al.*, 2006, 2005; *Lynch et al.,* 2004] and there is some evidence that reductions in sea ice may affect locations far from the Arctic [e.g., *Overland*, 2016], manifesting particularly through extreme weather in the mid-latitudes [e.g., *Cohen et al.*, 2014; *Francis and Vavrus*, 2012].

The distribution of the age of Arctic sea ice contributes to the vulnerability of the ice cover during the melt season because older ice is on average thicker than younger ice [*Tschudi et al.*, 2016]. Younger ice is more susceptible to deformation and melts out more readily during the summer, whereas older ice is more likely to remain through the melt season if it does not advect out of the Arctic Ocean. The pre-melt fractional distribution of ice age may therefore serve as a descriptive predictor of how much sea ice will disappear during the melt season and indicate where summer ice loss is more likely to occur.

Ice thickness observations are becoming more widely and readily available from satellite altimeters such as NASA's Ice, Cloud, and land Elevation Satellite (ICESat) [*Kwok and Cunningham*, 2008] and ESA's CryoSat-2 [*Laxon et al*., 2013; *Kurtz et al*., 2014]. However, these satellite-derived data cover a limited time span. ICESat collected twice-yearly monthly estimates from 2003 to 2008 and CryoSat-2, launched in 2010, produces complete Arctic-wide fields monthly [*Tilling et al*., 2016]. The laser altimeter on NASA ICESat-2, launched in September 2018 [*Markus et al*., 2017], provide a significant new source of snow+ice freeboard, and potentially thickness. Along with satellite-borne altimeters, NASA's Operation IceBridge has yielded thickness estimates during 2009 through 2019 in selected regions [e.g., *Kurtz et al*., 2013]. Submarine upward-looking sonar has also been used to estimate thickness sporadically since the 1950s over a selected region in the central Arctic. These data have been connected to the satellite altimetry record [*Kwok*, 2018] to create an intermittent long-term timeseries over part of the Arctic. While these direct ice thickness estimates are useful, such products lack the long-term and/or the basin-wide coverage that is available from the multi-decadal sea ice age record.

In contrast, sea ice motion can be used to track parcels in a Lagrangian sense and record their age. Several sea ice motion products have been developed by various groups. Most products use some sort of motion tracking approach to estimate the drift of features or patterns in satellite images. The EUMETSAT Ocean and Sea Ice Satellite Application Facility (OSI SAF) has two products. One is a low-resolution (62.5 km spacing) product that derives 2-day motions based on passive microwave and scatterometer inputs [*Lavergne et al*., 2010]. A medium resolution OSI SAF product based on visible/infrared sensor inputs provides daily coverage at 20 km spatial resolution [*Dybkjaer*, 2018]. Another product, developed by the

French National Institute for Ocean Science (IFREMER), combines passive microwave and scatterometer inputs to produce 3-day motion estimates [*Girard-Arduin and Ezraty*, 2012].

In this paper, we specifically discuss the "Polar Pathfinder Daily 25 km EASE-Grid Sea Ice Motion Vectors" product [*Tschudi et al*., 2019a]. These sea ice motions derived from satellite instruments and buoys are then used to obtain a continuous, complete, long-term record of sea ice age, the "EASE-grid Sea Ice Age" product [*Tschudi et al.*, 2019b]. Because of its length and completeness, this ice age timeseries has been used in several studies [*Maslanik et al.*, 2007, 2011; *Tschudi et al.*, 2016; 2010] and reviews of Arctic change [*Stroeve et al.*, 2011; *Meier et al.*, 2014; *Perovich et al.*, 2018] to assess changes in the ice cover. Over time, enhancements and improvements have been made to the ice motion and ice age products. The latest version of the ice age product addresses issues noted by users [*Szanyi et al.*, 2016] and both products are enhanced through a refined optimal interpolation approach that improves the spatial continuity of the gridded motion and age fields. Our focus in this paper is to highlight the changes in the new version, compare the new version with older versions, and provide an updated assessment of ice age trends. As further background, we also document the algorithms and production of the products. Because the ice age product is produced by utilizing the sea ice motion product, we outline the production of the motion product first.

2 The Polar Pathfinder Sea Ice Motion Product

The sea ice motion product is archived and distributed by the NASA Snow and Ice Distributed Active Archive Center (DAAC) at the National Snow and Ice Data Center (NSIDC). The ice motion product provides gridded daily estimates and weekly and monthly averages of ice motions for both the Arctic and Antarctic regions. In this section, we describe the basic processing methodology and data sources, as well as noting the changes made in the new Version 4 of the product. The version history of the motion product (and the age product discussed in Section 3) is summarized in Table 1, including the release date and enhancements for each version.

2.1 Sea ice motion data sources and derivation techniques

Here we provide an overview of the source data and the basic derivation approach. Further details are provided in the product User Guide, available at NSIDC (https://nsidc.org/data/nsidc-0116). There are three primary types of sources for the sea ice motion product: (1) gridded satellite imagery – from several sources, (2) winds from reanalysis fields, and (3) buoy position data. Motions are independently derived from each of these sources. A list of the sources, temporal coverage, and spatial resolution is provided in Table 2. A complete daily gridded product is then produced by combining all sources via an optimal interpolation scheme (Figure 1), which is described further below.

Gridded satellite imagery

The approach used for deriving ice motion from satellite imagery is a pattern-matching method that uses cross correlations between patterns in coincident images separated by a given time interval. Such an approach is commonly called "feature-tracking", but at the spatial scales for these images, it is a spatial pattern of many features that are being tracked. Specifically, for our product, motion vectors are computed using a maximum cross-correlation (MCC) pattern-matching method [*Emery et al.*, 1991, 1995]. Two geolocated, spatially-coincident, temporally-consecutive satellite images are selected. Typical time separation between images is 1 to 3 days. For each valid sea ice grid cell, a "search window" is defined for a region around that grid cell, sized so that it will encompass the range of potential motion during the prescribed time interval (typically ~50 km). The later image is translated relative to the earlier image within this search window, and the correlation between the two images is calculated for each translation. The highest correlation value, i.e., the correlation peak, is determined to be the offset in the position of the grid cell between the earlier and the later image; then, the ice velocity is computed by dividing this offset by the time separation between images.

The imagery sources have changed over time, depending on which inputs have been available. The primary source has been passive microwave imagery from a series of sensors. Horizontal and vertical polarization fields of 37 GHz and 85 GHz channels are used when available. These began in late 1978

with the Scanning Multichannel Microwave Radiometer (SMMR) on the NASA Nimbus-7 platform, which operated until August 1987. After SMMR, a series of Special Sensor Microwave Imagers (SSMI) on U.S. Defense Meteorological Satellite Program (DMSP) platforms carried on the time series. These were used for the motion product through 2006. Starting in 2007, the motion product transition to the DMSP successor instrument, the Special Sensor Microwave Imager and Sounder (SSMIS), of which three still continue to operate (as of February 2019). The SSMI and SSMIS imagery are derived from the DMSP SSM/I-SSMIS Daily Polar Gridded Brightness Temperatures, Version 4 product [*Maslanik and Stroeve*, 2004] and the SMMR imagery are from the Nimbus-7 SMMR Polar Gridded Radiances and Sea Ice Concentrations, Version 1 product [*Gloersen*, 2006].

These SMMR-SSMI-SSMIS sources are useful because they provide complete daily coverage in all-sky conditions (i.e., including night and through clouds). However, their low spatial resolution (25 km gridded) limits the resolution of motion estimates that can be retrieved. For example, for the SSMI-SSMIS fields, with a gridded a resolution of 25 km, daily velocity can only be estimated to the nearest 25 km/day for each velocity component. For this reason, many similar motion products use image pairs separated by more than one day. However, our product obtains useful daily motions by applying an oversampling procedure – effectively moving the correlation window fractions of grid cells – to obtain sub-pixel resolution. During initial development of the motion algorithm, various oversampling intervals were evaluated for improvement in accuracy versus computational expense. Based on these empirical analyses, an oversampling of 4X was chosen and is applied to all satellite estimates. This improves the SSMI-SSMIS effective sampling interval to 6.25 km/day, which corresponds to a motion precision of 7.23 cm/s. The optimal interpolation method described below smooths this "discretized" motion allowing estimation of much slower motions.

In 2002, a more advanced passive microwave sensor, the NASA/JAXA Advanced Microwave Scanning Radiometer for the Earth Observing System (AMSR-E), was launched on the NASA Aqua satellite and operated until October 2011. AMSR-E had more than double the spatial resolution of the previous sensor, 6.25 km gridded resolution for some channels, so its motion resolution was likewise improved. So, during

this period (2002-2011), it was also used as a source for ice motions. In 2012, JAXA launched AMSR2 on their Global Change Observation Mission – Water (GCOM-W) satellite, which continues to operate (as of November 2019). AMSR2 has not yet been added as a source, but this is planned for a future release of the motion product.

For the period, 1981-2000, vectors were produced from the Advanced Very High Resolution Radiometer (AVHRR). AVHRR is a visible/infrared sensor that provides higher spatial resolution than the passive microwave sources. Daily gridded composites at 4 km resolution were used as input to the maximum cross-correlation algorithm. The higher resolution of the sensor provided more accurate motion estimates that the SMMR-SSMI record. However, motions could only be derived when there were cloud-free conditions on consecutive days. This yielded relatively few vectors, and the impact of AVHRR was relatively small. With the advent of AMSR-E, having similar spatial resolution (6.25 km vs. 4 km) as AVHRR, but with the advantage of all-sky capability resulting in far more motion estimates, inclusion of AVHRR as a motion source was discontinued after 2000.

To further reduce errors, post-processing filtering techniques are applied to the cross-correlation scheme. First, a minimum correlation threshold of 0.4 is applied. This removes 'weak' matches that are more likely to be incorrect. Various thresholds were investigated during the original development of the product and 0.4 was qualitatively determined to be optimal in terms of balancing the allowance of too many erroneous matches versus incorrectly removing many "good" matches. Second, a neighborhood filter is applied. At the low-resolution of the satellite data, motion is spatially well-correlated across several grid cells. Retrieved vectors that are not similar with at least two neighboring estimates are considered to be spurious and are rejected. These spurious vectors occur frequently near the ice edge.

Version 4 changes. There have been two significant changes made to the satellite imagery processing for Version 4. First, the final quality-controlled and calibrated gridded passive microwave brightness temperatures [*Maslanik and Stroeve*, 2004] have been used throughout the record. In previous versions, near-real-time gridded brightness temperatures [*Maslanik and Stroeve,* 1999] were used to augment the

time series and there was no provenance on when the near-real-time or final source was used. Another change corrected over-filtering of passive microwave vectors that removed valid motion estimates in Version 3 of the product. This over-filtering was due to improperly ignoring some vectors in the filtering process. This had a relatively small effect in the Arctic because the multiple motion sources provided nearby motion estimates to compensate for the lack of microwave estimates; however, in the Antarctic, where the passive microwave estimates provide the only motion information, the sparser motion estimates often resulted in unrealistic circulation patterns.

Reanalysis winds

The satellite imagery sources are augmented in the Arctic with motions derived from wind forcing using the NCEP/NCAR Reanalysis [*Kalnay et al*., 2016] on a roughly 2° x 2° latitude-longitude grid, which are interpolated to a 50 km EASE-Grid (see Table 2). Wind-derived motions are not currently used in the Antarctic. The ice motions estimates are derived based on a simple relationship between winds and ice motion. The sea ice is assumed to move in the geostrophic wind direction, as provided by the reanalysis fields, with a magnitude of 1% of the wind speed. This was implemented based on the estimate from *Thorndike and Colony* [1982]. Other studies have shown a higher percent (e.g., 2%) for the ice vs. wind speed relationship. Recent studies indicate that the ice is becoming more responsive to winds [e.g., *Spreen et al*., 2011]. So, the 1% value used here likely underestimates the wind-driven ice speed. However, no changes were made to the wind-derived motions for Version 4, though below we show that the combined motion fields is largely insensitive to the magnitude of the wind contribution because it has a relatively small weight compared to the other sources. In a future version, we plan to revisit this relationship in the Arctic and investigate adding wind-driven motions for the Antarctic.

Buoy positions

Ice motion vectors are also computed by incorporating position data from the network of drifting buoys deployed as part of the International Arctic Buoy Program [*IABP*, 2008]. These buoys monitor

meteorological and oceanographic conditions for real-time operational requirements and research purposes, and provide ice motion by transmitting updated locations. This product uses the twice daily (midnight and noon) locations of the IABP "C" buoy product. Two motion estimates are computed from these locations: one from noon of one day to noon of the following day, and one from midnight of a day to midnight the following day. No buoys are included in the Antarctic motion fields because there have been few buoy deployments on ice in the Southern Ocean.

Version 4 changes. The principal change for the buoys is how the twice-daily observations are integrated into a daily product. Previous versions of this product considered these motions independently of each other and effectively used the most recent observation for a day. In Version 4 the two estimates are averaged to provide one daily motion estimate for each buoy. Thus, each day's buoy motion is an average of midnight to midnight (UTC) of the current day and noon the previous day to noon the current day. Also, the IABP source product recently started including floatable buoys, resulting in motion estimates from off the ice. These were not screened out in earlier versions. The effect was relatively small and primarily influenced motions near the ice-edge because of the distance-weighting interpolation. Version 4 now applies an ice mask to the buoys, making the buoy motion domain consistent with the other sources.

Masks for valid motions

Two masks are applied to limit motion retrievals to only regions where sea ice exists. First, a modified land mask is applied. The standard land mask is "dilated" so that cells near land are also excluded because motion retrievals near the coast are unreliable due to the effects of mixed land and ice/ocean grid cells. Because of its narrow channels, the Canadian Archipelago region is also masked out.

Second, a sea ice mask is also applied to limit motion retrievals to only ocean regions that are ice-covered on the days under consideration. The mask is based on the "Sea Ice Concentrations from Nimbus-7 SMMR and DMSP SSM/I-SSMIS Passive Microwave Data, Version 1" at NSIDC [*Cavalieri et al.*,

1996]. The mask defines all areas with concentrations greater than 15% as ice-covered so that valid ice motions can be computed.

Version 4 changes. Previously, the sea ice mask from only the first day was used to define the valid motion region. This was changed in Version 4 to allow motions only where ice is present on both days used to retrieve motions. This results in very small changes near the ice edge. As noted above, the mask is now applied to buoys as well as the other sources.

2.2 Uncertainty of motion estimates

Errors in the ice motion and ice age products are dependent on the resolution of the satellite sensor, as well as geolocation and binning errors for each image pixel [*Meier et al.*, 2000]. The distance precision of motion detection is limited by the grid cell resolution – a pattern can nominally be "observed" to move only an integer number of grid cells. Particularly for the low-resolution inputs, this yields high uncertainty for each individual estimate and an overall noisy motion field.

As noted above, for a 25 km gridded input with 4X oversampling, the limit of precision of the motion is 7.23 cm/s. Atmospheric effects and temporal variability of the surface are additional sources of error, especially in the summer. However, several evaluation studies have found that in practice errors are often lower because the different sources of error offset each other. *Kwok et al*. [1998] compared ice motion estimated from the European Space Agency (ESA) Remote Sensing Satellite (ERS-1) synthetic aperture radar (SAR) along with drifting buoy motion to the Lagrangian motion product and found an error of 5-12 km/day (~6-14 cm/s). Meier et al. [2000], comparing with buoys, found RMS errors of SSMI-derived daily velocity components to vary between ~5-7 cm/s, depending on conditions, with near-zero bias. AMSR-E, with higher spatial resolution, has velocity component errors of 4-5 cm/s [*Meier and Dai*, 2006; *Kwok*, 2008]. *Sumata et al*. [2014] found a correlation coefficient of 0.94 and 0.87 when comparing the ice motion data to IABP buoy drift in winter and summer, respectively. Summertime drift error was higher due in part to surface melt, which affects the passive microwave identification of ice parcels. The largest

drift error is found in the fall, which is likely due to formation of new ice [*Meier et al*., 2000]. Optimal interpolation (discussed below) reduces errors through its error and distance-based weighting, particularly when buoys are incorporated. Temporal averaging further reduces errors in the weekly estimates.

In addition, the errors are not generally cumulative, because the motions have been found to be largely unbiased evaluations during the development of the original product. These evaluations, described in the product documentation at NSIDC (https://nsidc.org/data/nsidc-0116), show *u* velocity component biases of ~±0.05 cm/s and *v*-component biases of 0.4-0.7 cm/s. Other published studies (such as the references above) show similar results. The low bias in the estimates means that errors in long-term (weeks to months) displacement are relatively small. *Tschudi et al*. [2010] compared drift tracks composed from the sea ice motion product to the drift of the Surface Heat Budget of the Arctic Ocean (SHEBA) ice camp [*Uttal et al*., 2002] and found a drift error of 27 km over 293 days. There is some effect from the different passive microwave sources due to temporal sampling between SMMR (every other day) and SSMI/SSMIS (daily); the higher sampling rate from SSMI/SSMIS changes the discretization of the retrieved motions. Also, the higher spatial resolution of AMSR-E affects the discretization of the motions as well. This is discussed further in the validation section below. Ice motion estimates in the Antarctic are not easily validated due to the lack of buoys for comparison. Generally, Antarctic motions are considered to be less accurate due to the lack of buoys, the more dynamic nature of the Antarctic sea ice, and the larger variability in microwave emission (e.g., flooding and snow-ice formation), limiting the effectiveness of the cross-correlation scheme.

2.3 Combined gridded sea ice motion fields

Daily motion fields are provided from each of the sources during their period of availability. However, for many users, the most useful parameter is the combined gridded product. This combines via an optimal interpolation scheme all available sources for a given day onto a version of the 25 km EASE-Grid [*Brodzik et al.*, 2002]. For further information and the grid, see NSIDC's documentation for this data product [*Tschudi et* al., 2019a]. For each 25-km ice EASE-grid cell, the speeds (cm/s) in the EASE-grid x-

direction (u velocity component) and y-direction (v velocity component) are stored. The daily motions fields are also averaged into weekly and monthly fields.

Optimal interpolation (also called "kriging") is not simply a spatial average, but also considers the accuracy of different sources and the spatial distribution of the source estimates. The motion estimates vary in expected quality with buoys considered most accurate, followed by passive-microwave and/or AVHRR-based estimates and finally by the wind field. This weighting is of the form:

$$w = Ce^{(-d/D)} \quad (1)$$

where w is the weight, C is a source-based coefficient (0.45 for wind, 0.95 for buoy, 0.8 for other sources), d is the Euclidean distance between the pixel in question and the motion estimate on the EASE grid, and D is the length-scale (constant) over which the estimates are correlated. The values of C are constant for each source and are based on early comparisons between each source and buoy estimates. Buoys, being the most accurate, were assigned the 0.95 value and the other sources' C values were calculated relative to buoys. Thus, estimates that are closer (low d) and higher quality (sources with high C, e.g. buoys), are weighted higher. We assume that buoys are by far the most accurate motion source and are assigned a high C value of 0.95. We use the buoys as the baseline for estimating the other weights. The values of C for the other sources were estimated *a priori* based on comparisons between the source motions and buoy estimates. The correlation length-scale, D, was also estimated empirically, based on cross-correlations of estimates separated by varying distances. The method loops through all grid cells in the domain that are flagged as sea ice-covered. Figure 2 shows an example of the individual motion sources and the resulting combined motion field. The optimal interpolation converts the sparse and/or noisy individual motion fields into a complete and smoothly varying combined motion grid.

Version 4 changes. The most notable change in the motion product for Version 4 involves the optimal interpolation approach. In previous versions, the combined estimate at each valid grid cell was estimated by optimally interpolating (kriging) the surrounding 15 closest vectors. While this generally gives a good

spatial distribution around grid cells, it does not necessarily include all estimates that fall within correlation length-scale and that theoretically could influence the interpolated estimate. This means that discontinuities can potentially occur, particularly as highly-weighted estimates (i.e., buoys) fall off the list of closest estimates. When the buoy motion estimates differ significantly from other sources, artificially large spatial gradients in velocity magnitude can arise [*Szyani et al*., 2016]. In Version 4 of the product, the methodology has been revised to use the 15 highest-weighted ice motion vectors at each grid cell, regardless of source. This means that higher weighted observations have influence over a longer distance and their influence drops off more gradually. This approach significantly reduces and often removes the discontinuity artifact in the daily interpolated product (Figure 3).

As noted above, the Version 4 algorithm also eliminates an over-filtering of SSMI, SSMIS, and AMSR-E passive microwave vectors that occurred in Version 3. Since these vectors are the only source in the Antarctic, they are the only input to the optimal interpolation. The over-filtering of the vectors resulted in a sparse raw motion field. While the correlation length scale of sea ice motion is typically 800-1000 km, given the coarse spatial resolution and high noise in the daily passive microwave derived motion vectors, such few vectors do not provide a spatially representative sample of the large-scale motion circulation. In other words, the interpolated motion field of the Antarctic ice motion field was often being driven by very few underlying motion estimates, which led to unrealistic circulation patterns in the Antarctic because there were too few vectors to create a representative field. The effect also occurred in the Arctic but was much more limited because other sources exist to augment the passive microwave estimates. Version 4 corrects this over-filtering, yielding more passive microwave motion estimates over a broader area, particularly in the Antarctic. An example of this is shown in Figure 4 where the Version 3 product has very few vectors. In the eastern Weddell Sea, this results in southward onshore ice motion. This would be very unusual for the region and comparisons with winds (not shown) show that this motion is not realistic. Version 4 yields more source vectors that better represents the spatial variation in the region. The result is a general eastward circulation, which is more typical for the region and agrees with the wind field.

A final change in the motion product for Version 4 is that the data are now provided in NetCDF format, with daily files for each underlying motion field, e.g. SSMI, buoy and wind-driven motions – as well as files containing the daily combined (optimally interpolated) estimate and a weekly average sea ice motion. The self-describing file format provides improved metadata (including georeference information) and easier access for many users. In the daily combined field, an error estimate is included that gives the error from the optimal interpolation, which is a function of the number, spatial distribution, and quality of all input vectors interpolated at a given grid point. Flag values are used to denote potential low-quality interpolation due to lack of nearby vectors and/or vectors near the coast (where retrievals have higher errors). Because the passive microwave daily ice motions are at a coarse resolution, they tend to exhibit discretization effects at daily timescales. These effects are diminished in the weekly fields as day-to-day "noise" in the observations are averaged out over the seven days. Thus, the weekly sea ice motion fields are the recommended product for most applications; users of the daily product should recognize its limitations and use caution in interpreting features and changes in the daily fields. The NSIDC archive also provides browse imagery of the weekly sea ice motions (Figure 5), which has also been updated to improve visual appearance.

2.4 Validation of combined motion fields

The combined motions are validated in the Arctic through comparison with independent buoys from the CRREL Ice Mass Balance Buoy program [*Perovich et al*., 2019]. We compared estimates to 103 CRREL buoys from 2000-2016. The combined estimate closest to each CRREL buoy was selected for comparison; thus, each comparison was made generally within ~25 km. Some CRREL observations with erroneous velocities that were obviously too large were removed from the comparisons. This resulted in a total of nearly 26,000 observations from these buoys. The results (Table 3) show that biases are around -0.1 cm/s for the u-component and around -0.65 cm/s for the v-component. Most notably, the biases were slightly reduced in Version 4, indicating that the improvements in processing do result in improved accuracy of the motions. Similarly, the error standard deviations are around 4 cm/s for both velocity components and Version 4 reduces this error by ~0.3 cm/s over Version 3.

As noted above, for the wind forcing, we used a 1% scale factor for the ice speed relative to wind speed. Other assessments have shown that 2% may be more legitimate, especially in recent years with the observed increasing trend in ice speed. To investigate the potential effect of underestimating ice speed from winds in our product, we compared the combined motion fields with both 1% and 2% scale factors to the 2015 CRREL buoy observations. The results indicate very little effect due to wind speed (Table 4), which is expected since the weighting of the wind-driven motion is much lower than other sources. The comparison indicates that the magnitude of the bias changes little for the u-component, but actually increases for the v-component. The error standard deviations also increase, generally by ~0.2 cm/s. This suggests that 2% may be too large overall. Of course, the relationship between wind speed and ice motion is complicated and can be quite variable. It depends on the compactness of the ice cover, thickness, and wind direction relative to nearby coasts. We plan to investigate the relationship further in the future, both regionally (for different sea ice conditions) and temporally (to investigate the effect of the long-term trend toward increasing speeds).

3 The EASE-Grid Sea Ice Age Product

The EASE-Grid Sea Ice Age product [*Tschudi et* al., 2019b] builds upon the motion product and is also a popular dataset with over 650 unique users having accessed the data as of this writing [*NSIDC*, personal comm.]. Version 2 of the sea ice age data is also part of NASA's Making Earth System Data Records for Use in Research (MEaSUREs) dataset at NSIDC [*Anderson et al*., 2014]; however, the MEaSUREs product is not regularly updated and does not include the newest enhancements described here. Animations of motion and age have been posted on NOAA's ClimateWatch online magazine [2016] (http://www.climate.gov/news-features/videos/old-ice-arctic-vanishingly-rare), which had over 300 hits the first day of posting, as well as the NASA Scientific Visualization Studio (https://svs.gsfc.nasa.gov/4509). Sea ice age distributions and trends are described annually in the Arctic Report Card [*Perovich et al.*, 2018] and have been analyzed by *Maslanik et al.* [2007; 2011].

The Sea Ice Age product was introduced by *Fowler et al.* [2004] and described further by *Maslanik et al.* [2007; 2011], *Tschudi et al.* [2010], and *Stroeve et al.* [2011]. The ice age product algorithm estimates

the age (in years) of Arctic sea ice using input from the previously described sea ice motion product. Weekly averaged motions are used to reduce computational complexity and to temporally average discretization artifacts in the daily motion data. Also, the 25 km resolution motions are bilinearly interpolated to a 12.5 km resolution grid in order to provide finer granularity in the ice age fields.

At the beginning of the ice motion record, all parcels in the 12.5 km ice age grid are initialized with an age-class of "first-year ice", meaning ice that is less than 1 year old. These parcels are then treated as Lagrangian particles and are advected at weekly time steps with the motion product estimates. When two or more parcels merge into a grid cell, the age of that grid cell is represented as the age of the oldest parcel. Rarely, ice motion results in all parcels being advected out of a grid cell; when this occurs, a new parcel of "first-year ice" is initialized in that grid cell. During the week of the Arctic sea ice extent minimum, the age of all parcels is incremented by one year. At each time step, all parcels found within a grid cell that has an ice concentration of less than 15% are considered to have melted and are no longer considered in determining the ice age. Parcels are tracked for up to 16 years, after which they are no longer considered (such parcels are simply removed).

This approach does not consider new ice that may form within a grid cell because it retains only the oldest ice in its accounting. Thus, the product is effectively an estimate of the oldest ice in a given grid cell. Tracking of partial concentration of age categories can provide a more detailed picture of the ice cover [*Korosov et al.*, 2018] and is something we may consider for future versions.

The source motion data for the age product begin in 1978, with the age of all parcels initialized as first-year (0-1 years old) ice. Because the method tracks age over time, several years are needed to build up older ice categories. For this reason, the ice age product begins in 1984. The youngest ice age category is first-year ice (FYI), which is ice that is less than a year old. Similarly, second-year ice is one to two years old, and so on for older ice age categories. Ice older than 4 years (5^{th}-year and older ice) makes up a very small percentage of the ice cover, so depicting ice older than this category as a separate field in browse

imagery is not undertaken. Therefore, the ice age is frequently categorized as being of ages: 0-1 (i.e., FYI), 1-2, 2-3, 3-4, and more than 4 years old (i.e., 5th-year and older ice).

Version 4 changes. The primary changes in Version 4 of the ice age product result from the changes in the source ice motion products described above. The most substantial change addressed anomalous behavior in the motion and age fields documented by *Szanyi et al.* [2016]. They showed that discontinuities in the interpolated motion field, caused by sub-optimal interpolation of buoys with the other data sources, created artificial ice divergence and new ice formation in the Version 3 product. This potentially results in an underestimation of multi-year and an overestimation of first-year ice. The change in the interpolation weighting, described above, reduced this effect as seen in Figure 3, where the circular features surrounding the buoys where the buoy weight suddenly drops to zero resulting in a discontinuity where false divergence can occur. The new weighting scheme smooths that discontinuity and eliminates much of the false divergence. The effect of this change can be seen qualitatively in the age fields as less "speckling" of first-year ice interspersed within the multi-year ice pack; the age fields show a more realistic consolidated multi-year ice pack. Quantitatively, the net effect is less first-year ice (the "speckling" that results from the false divergence) and an increased amount of multi-year in Version 4 compared to Version 3 (Figure 6). This effect becomes much less noticeable during the latter part of the record. There are three reasons for this. First, there is less passive microwave coverage during the early SMMR period, so a sparser number of vectors, which will accentuate interpolation-induced artifacts in the data. Similarly, in the early part of the record, there were far fewer buoys, so the buoy interpolation discontinuities are more noticeable. In recent years, there are enough buoys such that the interpolation distances of neighboring buoys often overlap, so discontinuities with the passive microwave and wind fields are less common. Finally, there is simply much less multi-year ice in recent years, so the discontinuity effects are less frequent. A quantitative assessment of the version changes in the ice age product are discussed further in Section 4 below.

Two other minor changes to the ice age product have been introduced in Version 4. First, the week-numbering convention was slightly modified to be consistent with the motion weeks. Second, browse

imagery (Figure 6) was improved to explicitly show ice-covered ocean areas that are outside of the age and motion domain (e.g., the Canadian Archipelago).

Validation of sea ice age is difficult because there is no known suitable validation data set that can be used for a comparison. Here we primarily rely on the fact that the ice age product is directly derived from the ice motion product. Thus, the demonstrated improvement in the motion fields indicates that the age fields are also improved. This is particularly noticeable in the reduction of the circular features in the motion field, which reduces the "speckling" in the Version 4 age fields. While this is qualitative, we feel this does demonstrate an improvement in the age fields. A recent study [*Lee et al*., 2017] included the NSIDC ice age fields in a comparison with passive microwave ice age retrieval methods, including multiyear fraction from the NASA Team algorithm, the OSI-SAF ice type product [*Aaboe et al*., 2017], and a microwave emissivity approach. The spatial patterns of first-year and multi-year ice in the NSIDC age product matched well with the comparison products, showing that our age product is at least consistent with other approaches.

4 Trends and variability in Version 4 ice motion and age and comparison to Version 3

Here we evaluate how the changes from Version 3 to Version 4 of the products affect the long-term trends and variability in the sea ice age fields. We also provide updated motion age trends through 2017.

As seen in Figure 3, the change to Version 4 does noticeably affect parts of the daily fields in regions around buoys. Over a weekly period, the changes are less significant because the motions are smoothed out. The weekly average speed in the Arctic is generally faster in Version 4 than in Version 3 (Figure 7). During the SMMR part of the record, the differences are generally near-zero. For the SSMI and SSMIS period, the Version 4 motions are ~0.5 – 1.0 cm/s faster than Version 3. During 2002-2011 when AMSR-E is included, the speed difference is reduced with Version 4 speeds ~0.25 – 0.5 cm/s faster. This change in behavior reflects (1) the different temporal sampling of SMMR (every other day vs. daily) and (2) the higher spatial resolution from AMSR-E and their effects on the cross-correlation motion retrievals. The differences in the *u* and *v* motion components (not shown) have similar characteristics over the time series.

There is seasonal variation with larger differences during summer. This corresponds to overall faster speeds, as seen in the Version 4 weekly average speed timeseries (Figure 8) that show strong seasonal variability with speeds peaking during summer.

There is also interannual variability (Figure 8), some of which is related to the SMMR every-other-day sampling, resulting in slower speeds and less variability for the 1979 to 1987 period. Beyond that, there is an overall increasing trend in Arctic sea ice speed of 0.21 cm/s/decade in Version 4 versus 0.13 cm/s/decade in Version 3. The increasing speed is in general agreement with previous studies that noted a trend toward faster moving ice [e.g., *Spreen et al.*, 2011] and linked the trend to greater response to wind-forcing by a thinner ice cover.

The largest effect of the version change for ice age is, as noted above, the amount of multi-year ice in the early part of the record, particularly in the oldest ice categories. This is illustrated in the timeseries of ice age (Figure 9). Both versions show a strong decline in 4+ year old ice over the record, with a steep loss of old ice in the late 1980s through the mid-1990s, which is associated with a persistent positive mode of the Arctic Oscillation (AO) [*Rigor et al.*, 2002]. A positive AO results in increased drift from the Siberian coast and greater advection of ice out of the Arctic through Fram Strait, which serves to "drain" older ice out of the Arctic [*Rigor and Wallace*, 2004].

The change to Version 4 results in higher extent of the old ice in the early part of the record, where Version 4 extent of 5+ year old ice is on average 367,000 km^2 higher than Version 3 for the first five years (1984-1988) of the record. This is an effect of the improved interpolation weighting scheme and is a quantitative indication of the reduced "speckling" discussed earlier. However, the impact dissipates over time; during the last five full years of the record (2012-2016), the difference between Version 4 and Version 3 is only 42,000 km^2. The amelioration of the difference is likely due to two factors: (1) the transition from SMMR to SSMI-SSMIS and the resulting improved coverage; and (2) the increasing number of buoys over time. As noted above, the two-day SMMR separation does change the motion discretization and the spatial coverage. So, the relative effect of the buoys are greater during the SMMR era. And with fewer buoys,

there is little to no overlap in terms of the spatial weighting of the buoys and the sharp discontinuities when buoy weighting drops to zero is more pronounced. With daily data and better spatial coverage in SSMI, the differences between the two versions starts to decrease. This decrease continues as buoy coverage increases over the years. And with AMSR-E and its better spatial resolution added in 2002, the differences drop further. By 2005, there is very little difference between the two versions. Focusing on the week of 19-25 February, the larger differences between versions of 4+ year old ice compared to younger ice types is evident (Figure 10). The younger ice categories show smaller, generally negative differences (i.e., less younger ice in Version 4). Thus, the changes in Version 4 appear to improve the ice age fields by removing much of the artificial divergence noted in *Szanyi et al.* [2016], thereby reducing the amount of younger ice and increasing the amount of older ice. However, the impact of the version change decreases over time such that there little impact on the age distribution in recent years.

Both versions of the ice age field show a transition from one dominated by older ice to one dominated by younger ice (Figure 11). Interannual variability is evident in all ice age classes, particularly first-year ice, which is not surprising given the variability of the summer ice cover. Less variability is seen in older ice. Nonetheless, the decline in older ice is apparent during the late-1980s through the mid-1990s persistent positive mode of the Arctic Oscillation [*Rigor et al.*, 2002]. After 1994, there was some recovery in multi-year ice before beginning a significant decline after 2004. Linear trends are estimated for the Arctic Ocean region. This is a region bounded by the northern coasts of the continents, the Bering Strait, Fram Strait, and the ~20 E meridian between Svalbard and the Fennoscandian Peninsula. The total area of the region is ~7.8×10^6 km^2. Using this region excises areas where only first-year ice exists, so it focuses on the areas where there is variability in the ice age. There is a strong increasing trend in ice less than 1 year old (Table 5) and a similar decreasing trend in 4+ year old ice. Trends in the intermediate ages (1-4 years old) are smaller. This is partly due to smaller extents of these ages as well as the fact that ice transitions through these categories between the larger extents of the oldest and youngest ice.

5 Conclusions

New versions (4.0) of the sea ice motion [*Tschudi et al.,* 2019a] and sea ice age [*Tschudi et al.,* 2019b] datasets have been produced and are now available at NSIDC. Routine updates will regularly occur when the underlying data – buoy positions, brightness temperature fields and sea ice concentration fields – become available. This is expected to occur every few months.

Arctic sea ice motion vectors are currently constructed by merging motion vectors estimated using three sources: buoys, passive microwave satellite imagery, and winds. In the Antarctic, only the satellite imagery vectors are used. Sea ice age is produced using the weekly northern hemisphere sea ice motion product as input, tracking ice parcels and aging them each year if they neither melt nor advect out of the ice pack.

The most recent sea ice motion algorithm revision incorporates improvements such as an improved vector weighting scheme, corrections to passive microwave vectors, new browse imagery, and the underlying code base through the use of Python. Furthermore, the Version 4.0 upgrade addresses artifacts in the ice motion resulting from the interpolation, though these artifacts did not substantially affect the weekly sea ice motion or age fields.

We note the decrease in older sea ice over the ice age record, from the 1980's, when older ice constituted ~30% of the ice pack, to recent years, when older ice occupies less than 5% of the pack. *Tschudi et al.* [2016] compared ice age to ice thickness derived from ICESat [*Kwok et* al., 2009; *Kwok and Cunningham*, 2008] and NASA's IceBridge campaign [*Kurtz et al*., 2012, 2013]. They found that the thickness/age relationship has an approximate linear fit for the ICESat dataset, but that the relationship was much more variable for IceBridge, due to the Arctic basin-wide coverage of ICESat thickness data and the more limited areal coverage for IceBridge aircraft-acquired data. The relationship found between ice age and thickness for the basin-wide ICESat dataset suggests that the ice age product may be used as a general indication of the sea ice thickness distribution, and could be compared to other Arctic basin-wide sea ice thickness estimations, such as those from CryoSat-2 [*ESA CPOM*, 2015].

The ice age motion and age products are continuously being improved. We plan to utilize passive microwave imagery from the AMSR2 instrument aboard the GCOM-1 satellite in a future release of the motion product, which may reduce the error in motion, due to the improved higher spatial resolution of AMSR2 over SSMIS. We also plan to further improve the age product by categorizing the age distribution in each EASE grid cell, instead of retaining only the oldest ice age. Numerous other improvements in the sea ice motion and age products are also planned, pending support.

6 Acknowledgments

The authors thank the anonymous reviewers for their helpful reviews of this manuscript. Research for this manuscript is supported by the NASA Cryospheric Sciences Program, per award NNX16AQ41G, and NASA Snow and Ice Distributed Active Archive Center (DAAC) at NSIDC.

References

Aaboe, S., L-A Breivik, A. Sørensen, S. Eastwood and T. Lavergne: Ocean & Sea Ice SAF Global Sea Ice Edge and Type Product User's Manual. http://osisaf.met.no/docs/osisaf_cdop3_ss2_pum_sea-ice-edge-type_v2p2.pdf, 2017.

Anderson, M. R., Bliss, A. C., and Tschudi, M.: MEaSUREs Arctic Sea Ice Characterization 25 km EASE-Grid 2.0. Boulder, Colorado USA: NASA DAAC at the National Snow and Ice Data Center. doi:10.5067/MEASURES/CRYOSPHERE/nsidc-0532.001, 2014.

Brodzik, M. J. and Knowles, K. W.: EASE-Grid: A Versatile Set of Equal-Area Projections and Grids in M. Goodchild (Ed.) Discrete Global Grids. Santa Barbara, California USA: National Center for Geographic Information & Analysis, 2002.

Cavalieri, D. J., Parkinson, C. L., Gloersen, P. and Zwally, H. J.: Sea Ice Concentrations from Nimbus-7 SMMR and DMSP SSM/I-SSMIS Passive Microwave Data, Version 1. Boulder, Colorado USA. NASA National Snow and Ice Data Center Distributed Active Archive Center. doi: http://dx.doi.org/10.5067/8GQ8LZQVL0VL, 1996, updated yearly.

Cohen, J., and several co-authors, Arctic amplification and extreme mid-latitude weather, Nat. Geosci., 7, 627-637, 2014.

Comiso, J. C., Meier, W. N., and Gersten, R.: Variability and trends in the Arctic sea ice cover: Results from different techniques, J. Geophys. Res., 122, 6883-6900, doi:10.1002/2017JC012768, 2017a.

Comiso, J. C., Gersten, R. A., Stock, L. V., Turner, J., Perez, G. J. and Cho, K.: Positive trend in the Antarctic sea ice cover and associated changes in surface temperature, J. Climate, 30, 2251-2267, doi: 10.1175/JCLI-D-16-0408.1, 2017b.

Comiso, J.C.: Large Decadal Decline of the Arctic Multiyear Ice Cover. J. Climate, 25, 1176–1193. doi: 10.1175/JCLI-D-11-00113.1, 2012.

Comiso, J. C., Parkinson, C. L., Gersten, R. and Stock, L.: Accelerated decline in the Arctic sea ice cover, Geophys. Res. Lett., 35, L01703, doi:10.1029/2007GL031972, 2008.

Dybkjaer, G.: Algorithm Theoretical Basis Document for OSI SAF medium resolution sea ice drift product, OSI-407-a, Version 2.3, 25 pp., http://osisaf.met.no/docs/osisaf_ss2_atbd_sea-ice-drift-mr_v2p3.pdf.

Emery, W. J., Fowler, C. W., Hawkins, J. and Preller, R. H.: Fram Strait satellite image derived ice motions. J. Geophys. Res., 96, 4751–4768, doi: 10.1029/90JC02273, 1991.

Emery, W. J., Fowler, C. and Maslanik, J: Satellite remote sensing of ice motion, in *Oceanographic Applications of Remote Sensing*, ed. Motoyoshi Ikeda and Frederic W. Dobson. CRC Press, Boca Raton, FL, 1995.

ESA CPOM: European Space Agency, Centre for Polar Observation and Modeling Data Portal. Available online at http://www.cpom.ucl.ac.uk/csopr/seaice.html, 2015.

Fowler, C. F., Emery, W. J. and Maslanik, J. A.: Satellite-derived evolution of Arctic sea ice age: October 1978 to March 2003. IEEE Geo. Rem. Sens. Lett., doi: 10.1109/LGRS.2004.824741, 2004.

Francis, J. A., and Vavrus, S. J.: Evidence linking Arctic amplification to extreme weather in mid-latitudes, Geophys. Res. Lett., 39, L06801, doi:10.1029/2012GL051000, 2012.

Francis, J. A., Hunter, E., Key, J. R. and Wang, X.: Clues to variability in Arctic minimum sea ice extent. Geophys. Res. Lett., 32, L21501, doi:10.129/2005GL024376, 2005.

Francis, J. A., and E. Hunter, E: Clues to changes in Arctic summer-minimum sea ice extent. 14th Conference on Satellite Meteorology and Oceanography, Atlanta, GA, 28 January – 2 February, 2006, doi: 10.1029/2005GL024376, 2006.

F. Girard-Ardhuin and R. Ezraty: Enhanced Arctic sea ice drift estimation merging radiometer and scatterometer data, *IEEE Trans. Geosci. Rem. Sens.*, 50(7), 2639-2648, doi: 10.1109/TGRS.2012.2184124, 2012.

Gloersen, P.: Nimbus-7 SMMR Polar Gridded Radiances and Sea Ice Concentrations, Version 1. Boulder, Colorado USA. NASA National Snow and Ice Data Center Distributed Active Archive Center. doi: 10.5067/QOZIVYV3V9JP, 2006.

Huntington, H.P., Hamilton, L.C., Brunner, R., Lynch, A., Nicolson, C., Ogilvie, A.E.J. and Voinov, A.: Toward understanding the human dimensions of the rapidly changing arctic system: insights and approaches from five HARC projects, Reg. Environ. Change, 7:173-186, doi:10.1007/s10113-007-0038-0, 2007.

IABP. International Arctic Buoy Programme: updated periodically. Online at http://iabp.apl.washington.edu/index.html.

Johannessen, O.M., E.V. Shalina, and W.M. Miles, 1999: Satellite evidence for an Arctic sea ice cover in transformation. Science, 286, 1937-1939, doi: 10.1126/science.286.5446.1937, 2008.

Kalnay, E., Kanamitsu, M., Kistler, R., Collins, W., Deaven, D., Gandin, L., Iredell, M., Saha, S., White, G., Woollen, J. and Zhu, Y.: The NCEP/NCAR 40-year reanalysis project. Bull. Amer. Meteorol. Soc., 77(3), pp.437-471, doi: 10.1175/1520-0477(1996)077<0437:TNYRP>2.0.CO;2, 1996.

Korosov, A. A., Rampal, P., Pedersen, L. T., Saldo, R., Ye, Y., Heygster, G., Lavergne, T., Aaboe, S., and Girard-Ardhuin, F.: A new tracking algorithm for sea ice age distribution estimation, The Cryosphere, 12, 2073-2085, doi:10.5194/tc-12-2073-2018, 2018.

Kurtz, N., Studinger, M., Harbeck, J., Onana, V. and Farrell, S.: IceBridge Sea Ice Freeboard, Snow Depth, and Thickness, Version 1. Boulder, Colorado USA: NASA DAAC at the National Snow and Ice Data Center, doi: 10.5067/7XJ9HRV50O57, 2012, updated 2015.

Kurtz, N. T., Farrell, S. L., Studinger, M., Galin, N., Harbeck, J. P., Lindsay, R., Onana, V. D., Panzer, B., and Sonntag, J. G.: Sea ice thickness, freeboard, and snow depth products from Operation IceBridge airborne data, The Cryosphere, 7, 1035-1056, https://doi.org/doi:10.5194/tc-7-1035-2013, 2013.

Kurtz, N. T., Galin, N. and Studinger, M.: An improved CryoSat-2 sea ice freeboard retrieval algorithm through the use of waveform fitting, The Cryosphere, 8, 1217-1237, doi:10.519/tc-8-1217-2014, 2014.

Kwok, R., Schweiger, A., Rothrock, D. A., Pang, S. and Kottmeier, C.: Sea ice motion from satellite passive microwave imagery assessed with ERS SAR and buoy motions. J. Geophys. Res., 103 (C4), 8,191-8,214, doi: 10.1029/97JC03334, 1998.

Kwok, R.: Summer sea ice motion from the 18 GHz channel of AMSR-E and the exchange of sea ice between the Pacific and Atlantic sectors, Geophys. Res. Lett., 35, L03504, doi:10.1029/2007GL032692, 2008.

Kwok, R., and Cunningham, G. F.: ICESat over Arctic sea ice: Estimation of snow depth and ice thickness, J. Geophys. Res., 113, C08010, doi:10.1029/2008JC004753, 2008.

Kwok, R., Cunningham, G. F., Wensnahan, M., Rigor, I., Zwally, H.J. and Yi, D.: Thinning and volume loss of the Arctic Ocean sea ice cover: 2003–2008, J. Geophys. Res., 114, C07005, doi:10.1029/2009JC005312, 2009.

Kwok, R.: Arctic sea ice thickness, volume, and multiyear ice coverage: losses and coupled variability (1958-2018), *Env. Res. Letters*, 13, 105005, doi:10.1088/1748-9326/aae3ec, 2018.

Lavergne, T., Eastwood, S., Teffah, Z., Schyberg, H. and L.-A. Breivik: Sea ice motion from low resolution satellite sensors: an alternative method and its validation in the Arctic. J. Geophys. Res., 115, C10032, doi:10.1029/2009JC005958, 2010.

Laxon, S. et al.: CryoSat-2 estimates of Arctic sea ice thickness and volume, Geophys. Res. Lett., 40, 1-6, doi:10.1002/GRL.50193, 2013.

Lee, S.-M., Sohn, B.-J., and Kim, S.-J.: Differentiating between first-year and multiyear sea ice in the Arctic using microwave-retrieved emissivities, J. Geophys. Res., 122, 5097-5112, doi:10.1002/2016JD026275.

Lynch, A. H., Curry, J. A., Brunner, R. D., and Maslanik, J. A.: Towards an integrated assessment of the impacts of extreme wind events on Barrow, Alaska. Bull. Amer. Meteorol. Soc., 85, 209–221, doi: 10.1175/BAMS-85-2-209, 2004.

Markus, T., and several co-authors: The Ice, Cloud, and land Elevation Satellite-2 (ICESat-2): Science requirements, concept, and implementation, Rem. Sens. Environ., 190, 260-273, doi:10.1016/j.res.2016.12.029, 2017.

Maslanik, J., Stroeve, J., Fowler, C. and Emery, W.: Distribution and trends in Arctic sea ice age through spring 2011. Geophys. Res. Lett., 38, L13502, doi:10.1029/2011GL047735, 2011.

Maslanik, J.A., Fowler, C., Stroeve, J., Drobot, S., Zwally, J., Yi, D. and Emery, W.: A younger, thinner Arctic ice cover: Increased potential for rapid, extensive sea-ice loss, Geophys. Res. Lett., 34, L24501, doi:10.1029/2007GL032043, 2007.

Maslanik, J. and Stroeve, J.: *DMSP SSM/I-SSMIS Daily Polar Gridded Brightness Temperatures, Version 4*. Boulder, Colorado USA. NASA National Snow and Ice Data Center Distributed Active Archive Center. https://doi.org/10.5067/AN9AI8EO7PX0, 2004.

Maslanik, J. and Stroeve, J.: Near-Real-Time DMSP SSMIS Daily Polar Gridded Sea Ice Concentrations, Version 1. Boulder, Colorado USA. NASA National Snow and Ice Data Center Distributed Active Archive Center. https://doi.org/10.5067/U8C09DWVX9LM, 1999, updated daily.

Meier, W. N., Maslanik, J. A. and Fowler, C. W.: Error analysis and assimilation of remotely sensed ice motion within an Arctic sea ice model, J. Geophys. Res., 105(C2), 3339–3356, doi:10.1029/1999JC900268, 2000.

Meier, W.N. and Dai, M.: High-resolution sea-ice motions from AMSR-E imagery, Ann. Glaciol., 44, 352-356, doi: 10.3189/172756406781811286, 2006.

Meier, W. N., et al.: Arctic sea ice in transformation: A review of recent observed changes and impacts on biology and human activity, Rev. Geophys., 51, 185–217, doi:10.1002/2013RG000431, 2014.

NOAA's Climate Watch: Available online at http://www.climate.gov/news-features/videos/old-ice-arctic-vanishingly-rare, 2016.

Overland, J. E.: A difficult Arctic science issue: Midlatitude weather linkages, Polar Science, 10, 210-216, doi:10.1016/j.polar.2016.04.011, 2016.

Parkinson, C. L., and Cavalieri, D. J.: Antarctic sea ice variability and trends, 1979-2010. The Cryosphere, 6, 871–880, doi: 10.5194/tc-6-871-2012, 2012.

Perovich, D., Meier, W., Tschudi, M., Farrell, S., Hendricks, S., Gerland, S., Haas, C., Krumpen, T., Polashenski, C., Ricker, R., Webster, M.: *Sea Ice* in [Arctic Report Card 2018], https://www.arctic.noaa.gov/Report-Card, 2018.

Perovich, D., J. Richter-Menge, and C. Polashenski, Observing and understanding climate change: Monitoring the mass balance, motion, and thickness of Arctic sea ice, http://imb-crrel-dartmouth.org/archived-data, 2019.

Pizzolato, L., Howell, S. E. L., Dawson, J., Laliberté, F. and Copland, L.: The influence of declining sea ice on shipping activity in the Canadian Arctic, *Geophys. Res. Lett.*, 43, doi:10.1002/2016GL071489, 2016.

Rigor, I.G., Wallace, J. M. and Colony, R. L.: Response of sea ice to the Arctic Oscillation, *J. Climate*, 15, 2648-2663, doi:10.1175/1520-0442(2002)015<2648:ROSITT>2.0.CO;2, 2002.

Rigor, I.G., and Wallace, J. M.: Variations in the age of Arctic sea-ice and summer sea-ice extent, *Geophys. Res. Lett.*, 31, L09401, doi:10.1029/2004GL019492, 2004.

Spreen, G., Kwok, R. and D. Menemenlis, D.: Trends in Arctic sea ice drift and role of wind forcing: 1992-2009, *Geophys. Res. Lett.*, 38, L19501, doi:10.1029/2011GL048970, 2011.

Stroeve, J., Barrett, A., Serreze, M. and Schweiger, A.: Using records from submarine, aircraft and satellites to evaluate climate model simulations of Arctic sea ice thickness, *The Cryosphere*, 8(5), 1839-1854, doi:10.5194/tc-8-1839-2014, 2014.

Stroeve, J. C., Serreze, M. C., Kay, J. E., Holland, M. M., Meier, W. N. and Barrett, A. P.: The Arctic's rapidly shrinking sea ice cover: A research synthesis, *Climatic Change*, doi:10.1007/s10584-011-1010-1, 2011.

Sumata, H., Lavergne, T., Girard-Ardhuin, F., Kimura, N., Tschudi, M. A., Kauker, F., Karcher, M. and Gerdes, R.: An intercomparison of Arctic ice drift products to deduce uncertainty estimates, *J. Geophys. Res. Oceans*, 119, 4887–4921, doi:10.1002/2013JC009724, 2014.

Szanyi, S., Lukovich, J. V., Barber, D. G., and Haller, G.: Persistent artifacts in the NSIDC ice motion data set and their implications for analysis, *Geophys. Res. Lett.*, 43, 10,800–10,807, doi:10.1002/2016GL069799, 2016.

Thorndike, A. S., and Colony, R.: Sea ice motion in response to geostrophic winds, *J. Geophys. Res.*, 87(C8), 5845–5852, doi:10.1029/JC087iC08p05845, 1982.

Tilling, R.L., Ridout, A. and Shepherd, A.: Near-real-time Arctic sea ice thickness and volume from CryoSat-2, *The Cryosphere*, 10, 2003–2012, doi:10.5194/tc-10-2003-2016, 2016.

Tschudi, M., W. N. Meier, J. S. Stewart, C. Fowler, and J. Maslanik: Polar Pathfinder Daily 25 km EASE-Grid Sea Ice Motion Vectors, Version 4. Boulder, Colorado USA. NASA National Snow and Ice Data Center Distributed Active Archive Center. doi: https://doi.org/10.5067/INAWUWO7QH7B, 2019a.

Tschudi, M., W. N. Meier, J. S. Stewart, C. Fowler, and J. Maslanik. 2019. EASE-Grid Sea Ice Age, Version 4. Boulder, Colorado USA. NASA National Snow and Ice Data Center Distributed Active Archive Center. doi: https://doi.org/10.5067/UTAV7490FEPB, 2019b.

Tschudi, M.A., J.C. Stroeve, J. C. and Stewart, J. S.: Relating the Age of Arctic Sea Ice to its Thickness, as Measured during NASA's ICESat and IceBridge Campaigns. *Remote Sens.*, 8(6), 457, doi: 10.3390/rs8060457, 2016.

Tschudi, M.A., Fowler, C, Maslanik, J.A. and Stroeve, J.C.: Tracking the movement and changing surface characteristics of Arctic sea ice. *IEEE J. Selected Topics in Earth Obs. And Rem. Sens.*, 10.1109/JSTARS.2010.2048305, 2010.

Uttal, T., et al.: Surface Heat Budget of the Arctic Ocean. *Bull. Amer. Meteor. Soc.*, 83, 255–275, doi: 10.1175/1520-0477(2002)083<0255:SHBOTA>2.3.CO;2, 2002.

Vermaire, J. C., Pisaric, M. F. J., Thienpont, J.R., Mustaphi, C. J., Kokelj, S. V., and Smol, J. P.: Arctic climate warming and sea ice declines lead to increased storm surge activity, *Geophys. Res. Lett.,* 40, 1386–1390, doi:10.1002/grl.50191, 2013.

Table 1. Version histories of the sea ice motion and age products.

Version	NSIDC Release Date	Motion	Age
1	Not distributed by NSIDC	Original version based on SMMR, SSMI, and AVHRR imagery, and buoy motions	Original research product
2	Sep 2013 (motion) Dec 2014 (age)	• Added AMSR-E sources • Added NCEP/NCAR wind-derived motions for Arctic	• First version distributed at NSIDC (as Version 2) • Used Version 2 ice motion product as input
3	Feb 2016	• Removed erroneous buoy and AVHRR-derived motions • Updated buoys motions through most recent date • Derived sea ice mask from NSIDC* product instead of internally derived concentration estimates • Used GDAL** library to interpolate SSMI fields from polar stereographic to EASE grid • Improved browse images	• Used Version 3 ice motion as input • Improved browse images
4	Nov 2018	• Used highest-weighted vectors for interpolated gridded fields instead of nearest vectors • Daily buoy motions averaged instead of using latest observation • Open water buoys removed • Final quality-controlled SSMI and SSMIS brightness temperatures used throughout record • Corrected over-filtering of SSMI and SSMIS vectors that had removed valid motion • Improved browse images	• Used Version 4 ice motion input • Updated week-numbering convention to be consistent with motions • Improved browse images

*Cavalieri et al., 1996; **Geospatial Data Abstraction Library (https://gdal.org).

Table 2. Temporal coverage of input source data, as of Nov. 2019. The products will be updated approximately yearly. Buoy motions are from GPS location data. *NCEP-NCAR winds are on T62 Gaussian grid, which ~100 km in the latitudinal direction, with variable longitudinal spacing.

Data	Source	Temporal Range	Source Resolution (km)	Gridded Motion Resolution (km)
Daily Sea Ice Motions	Interpolated from input data	01 Nov1978 – 31 Dec 2018		25
Weekly Sea Ice Motions	Averaged from Daily Sea Ice Motions	05 Nov1978 – 31 Dec 2018		25
Input Data	AMSR-E	19 Jun 2002 – 08 Aug 2011	6.25, 12.5	37.5
	AVHRR	24 Jul 1981 – 31 Dec 2000	5	50
	IABP Buoys	18 Jan 1979 – 31 Dec 2018	NA	NA
	NCEP/NCAR U-wind and V-wind	25 Oct 1978 – 31 Dec 2018	~100*	50
	SMMR	25 Oct 1978 – 08 Jul 1987	25	75
	SSM/I	09 Jul 1987 – 31 Dec 2006	12.5, 25	75
	SSMIS	01 Jan 2007 – 31 Dec 2018	12.5, 25	75

Table 3. Validation statistics from comparison with CRREL buoys.

	u-component (cm/s)	v-component (cm/s)
Bias		
Version 3	-0.114	-0.677
Version 4	-0.109	-0.651
Error St. Dev.		
Version 3	4.20	4.30
Version 4	3.91	4.01

Table 4. Comparison with CRREL buoys of combined motions using different wind-speed scaling.

	u-component (cm/s)	v-component (cm/s)
Bias		
1% of wind speed	-0.466	-0.623
2% of wind speed	-0.460	-0.697
Error St. Dev.		
1% of wind speed	4.63	4.41
2% of wind speed	4.80	4.55

Table 5. Linear trends for ice ages over three periods. The main values are for Version 4, with Version 3 values in italics on the line below. These values are for the Arctic Ocean region.

Sea ice age	1984-2017 Trend [km^2/year]	1984-1996 Trend [km^2/year]	1997-2017 Trend [km^2/year]
0-1	**69,200** ***(67,700)***	**96,200** ***(94,000)***	**92,500** ***(95,600)***
1-2	**10,500** ***(4,900)***	**22,100** ***(18,000)***	**4,500** ***(-3,500)***
2-3	**-4,900** ***(-7,300)***	**10,000** ***(2,000)***	**-12,500** ***(-11,900)***
3-4	**-10,100** ***(-11,200)***	**-11,400** ***(-9,000)***	**-16,100** ***(-16,700)***
4+	**-75,500** ***(-64,800)***	**-104,100** ***(-91,000)***	**-93,300** ***(-88,000)***

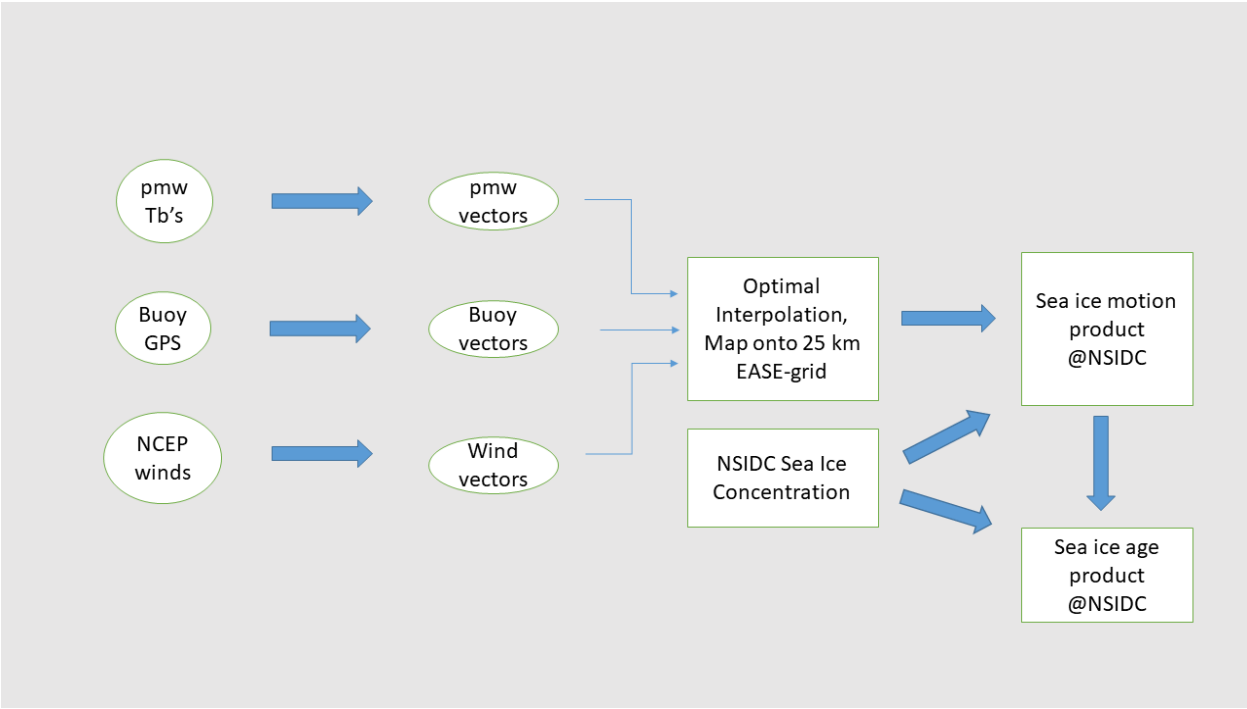

Figure 1. Flow chart for the production of the sea ice motion and age products.

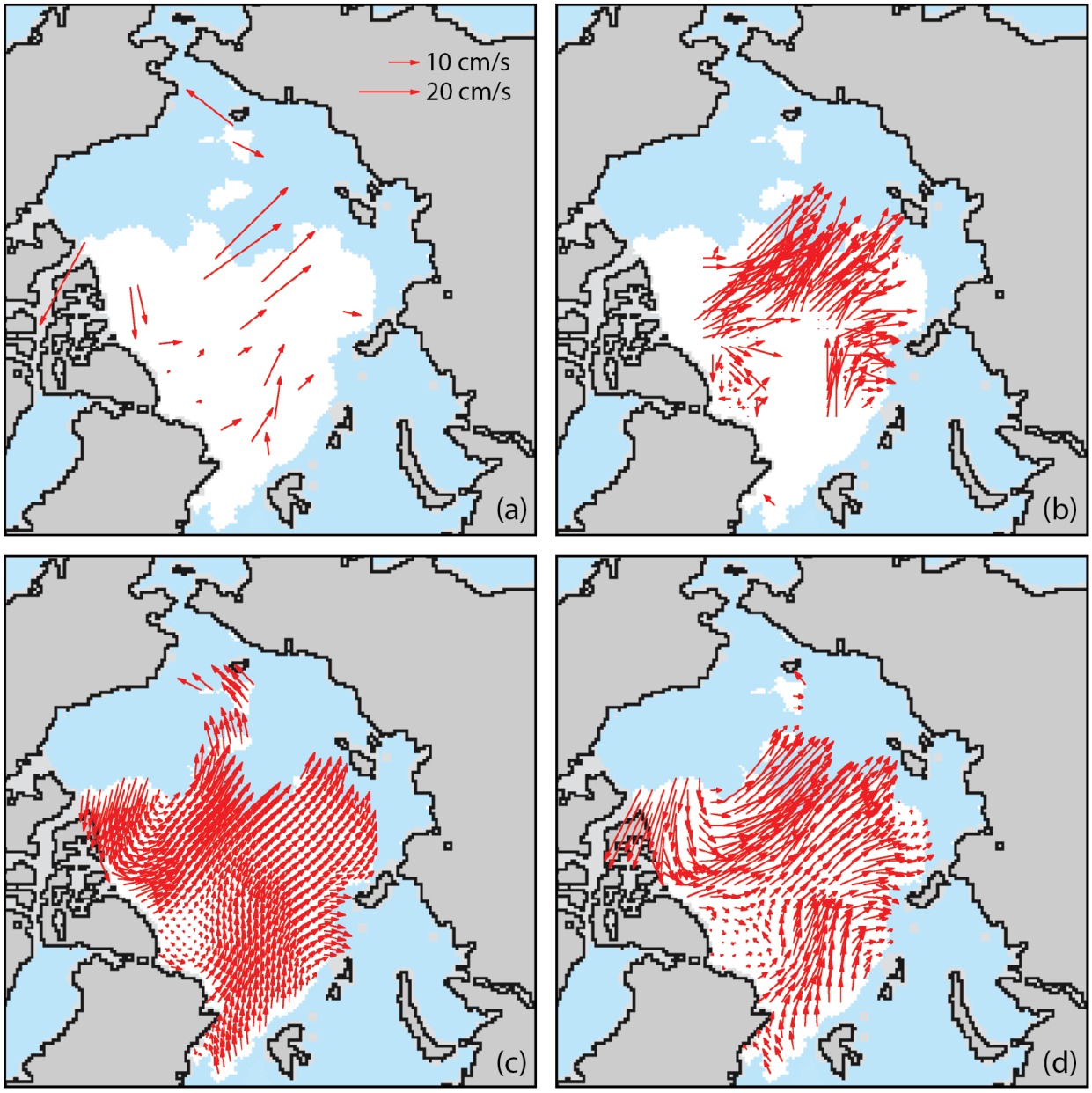

Figure 2. September 16, 2016 daily motion vectors from (a) buoys, (b) passive microwave, and (c) winds. The three sources are then merged to form (d) the daily interpolated sea ice motion field. Sea ice (white), ice-free ocean (blue), land (gray) and coast (black) are also shown. All buoys are shown, but other fields show only every 4th vector for legibility.

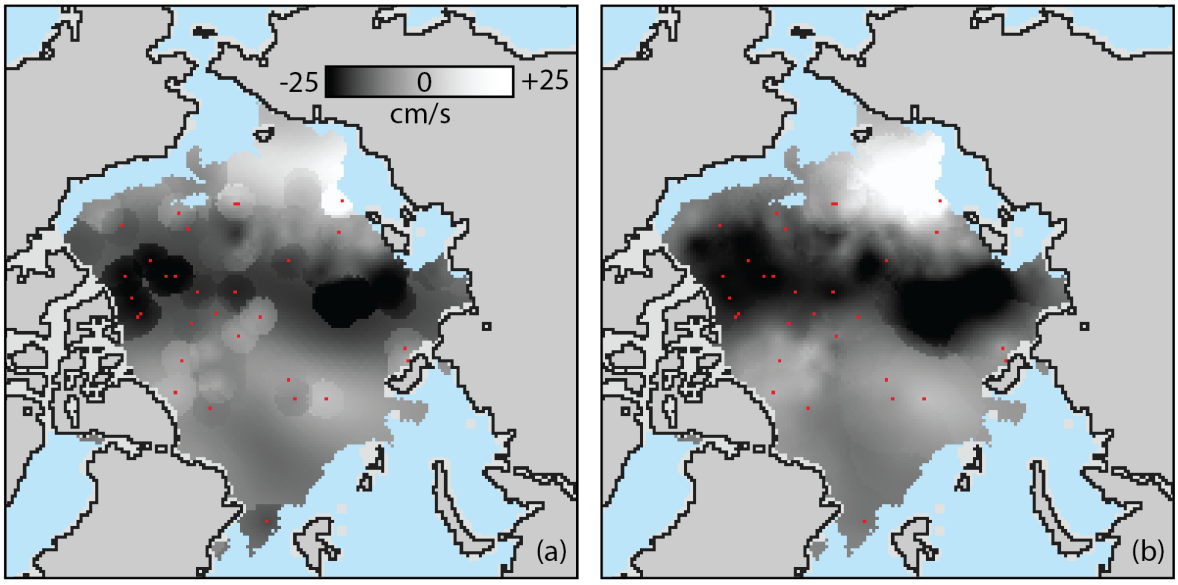

Figure 3. U-component of the daily interpolated vector field for September 17, 2001 from (a) Version 3 and (b) Version 4. The Version 3 fields show sharp gradients in the velocity when highly-weighted buoy estimates – buoy locations shown with red dots – no longer contribute to the motion field. Version 4 removes these sharp gradients by considering the highest weighted - rather than closest - underlying estimates.

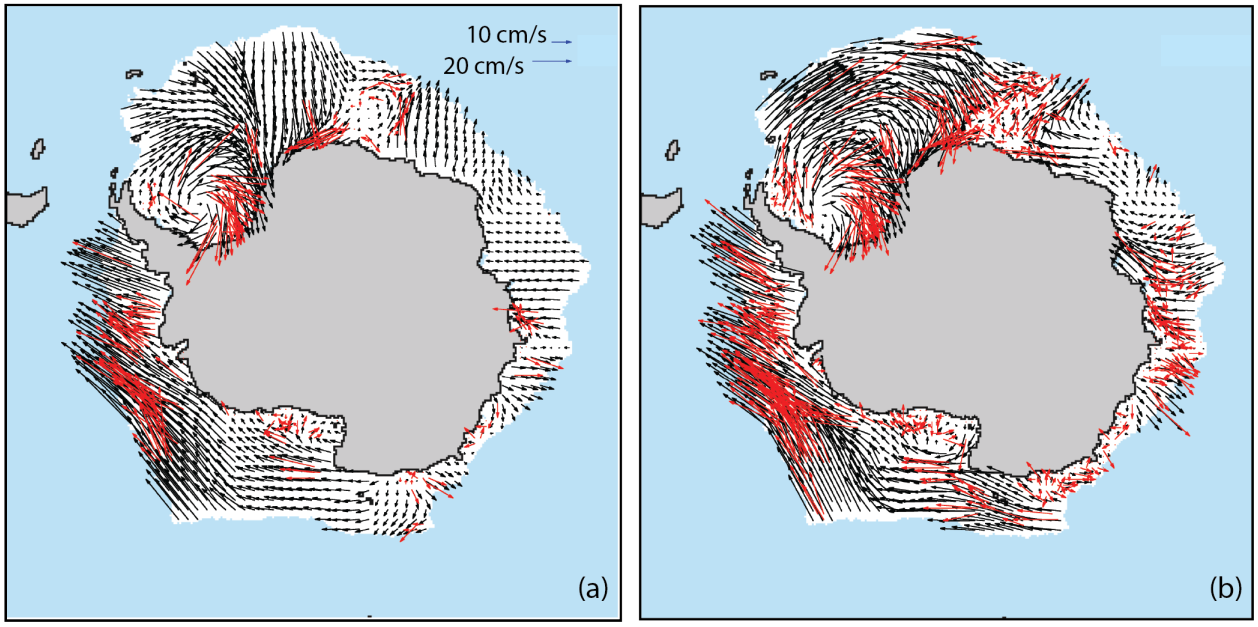

Figure 4. Version 3 (a) and Version 4 (b) Antarctic SSMI vectors (red) and resulting interpolated vectors (black) for August 22, 2001. Version 3 over-filtered the number of underlying SSMI vectors, often resulting in an ice field constructed from very sparse underlying data. Version 4 corrected this and includes more SSMI vectors. Every 4th vector is plotted for easier legibility.

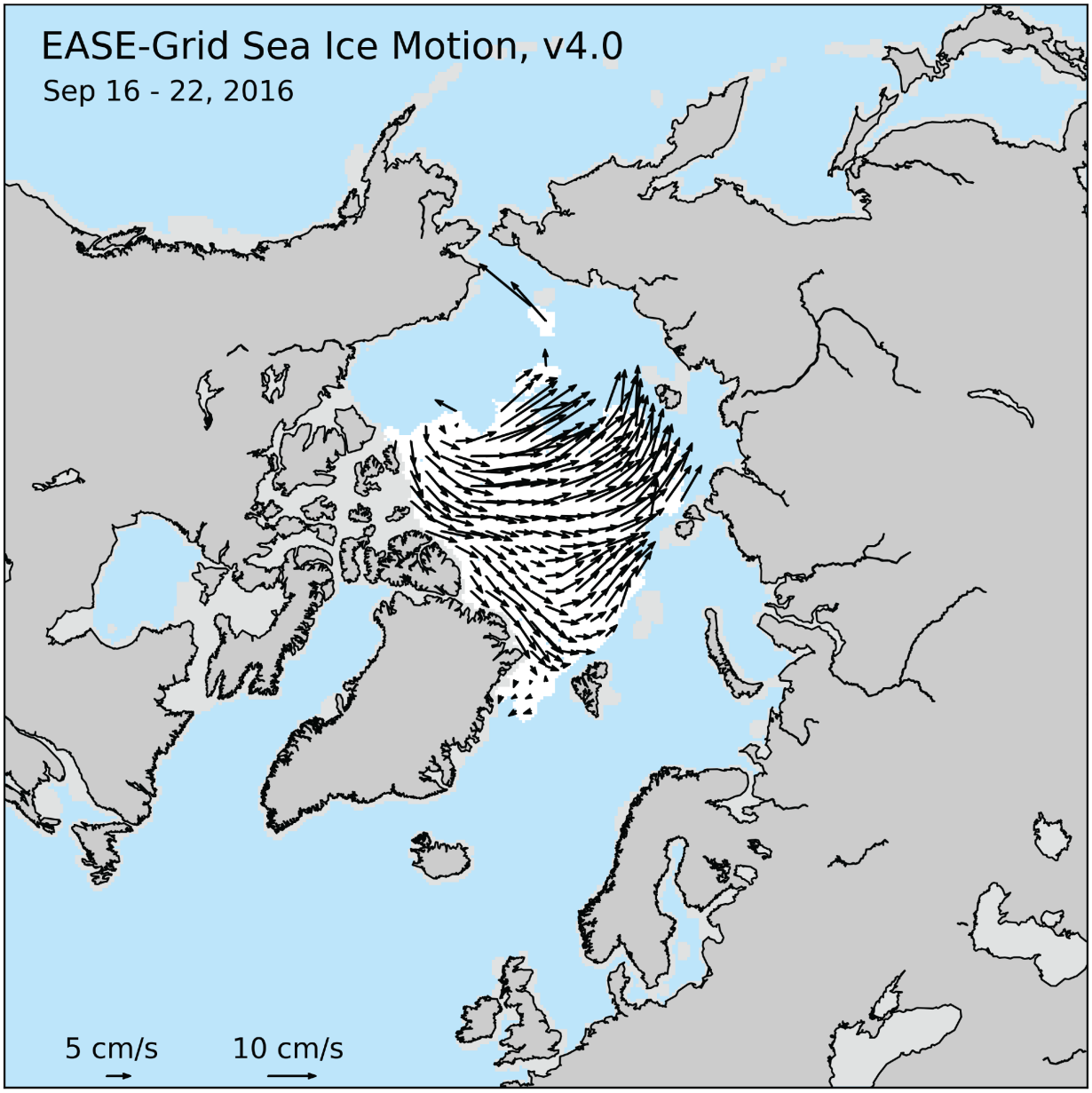

Figure 5. Example EASE-Grid sea ice motion for the Arctic region, the week of September 16-22, 2016. White indicates the sea ice mask region (>15% concentration). Note that motions are not retrieved in the Canadian Archipelago region or near coasts. Every 4th vector is plotted for easier legibility.

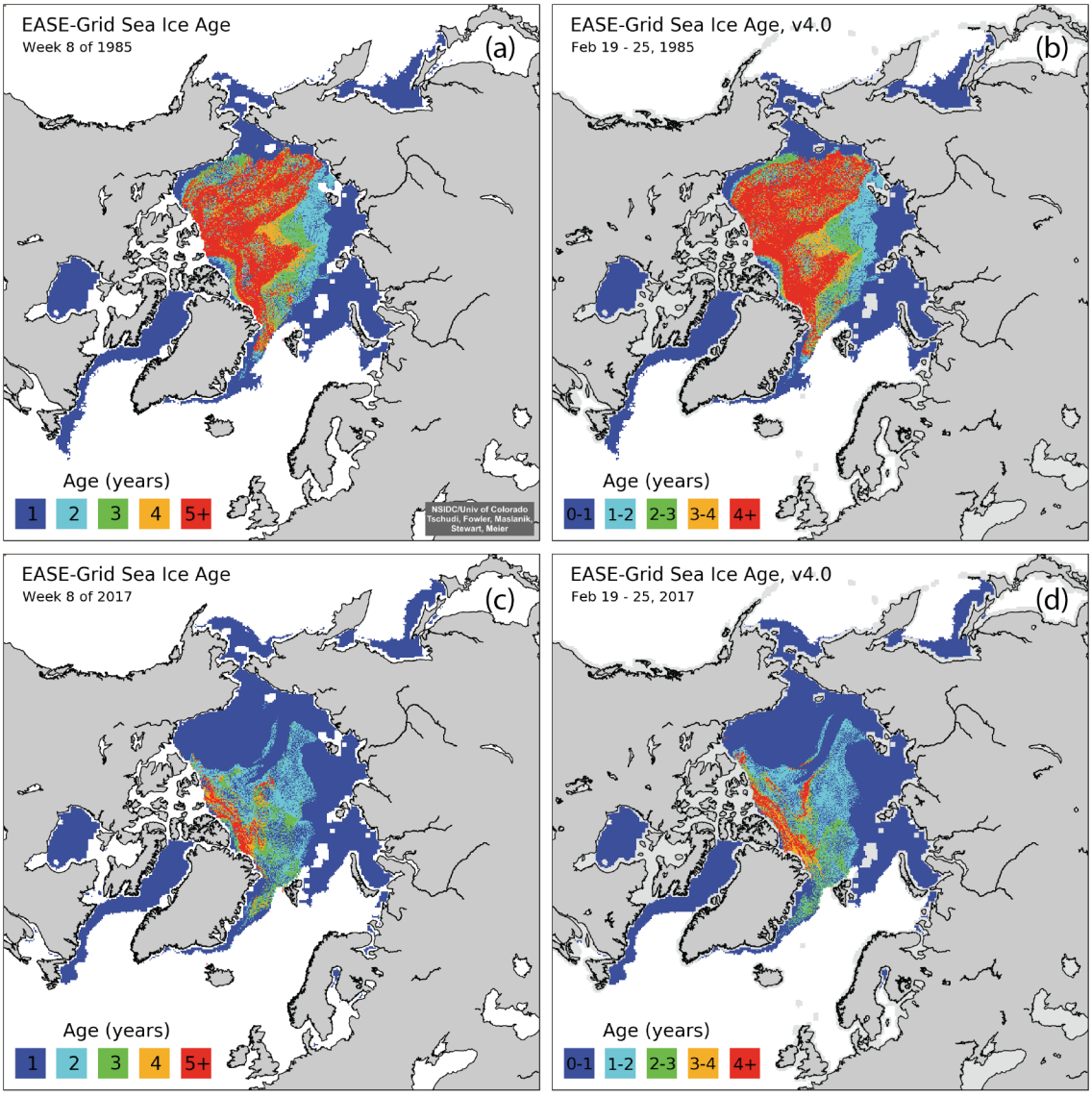

Figure 6. Comparison of Week 8 (Feb 19-25) ice ages for 1985 (a) Version 3 and (b) Version 4, and for 2017 (c) Version 3 and (d) Version 4.

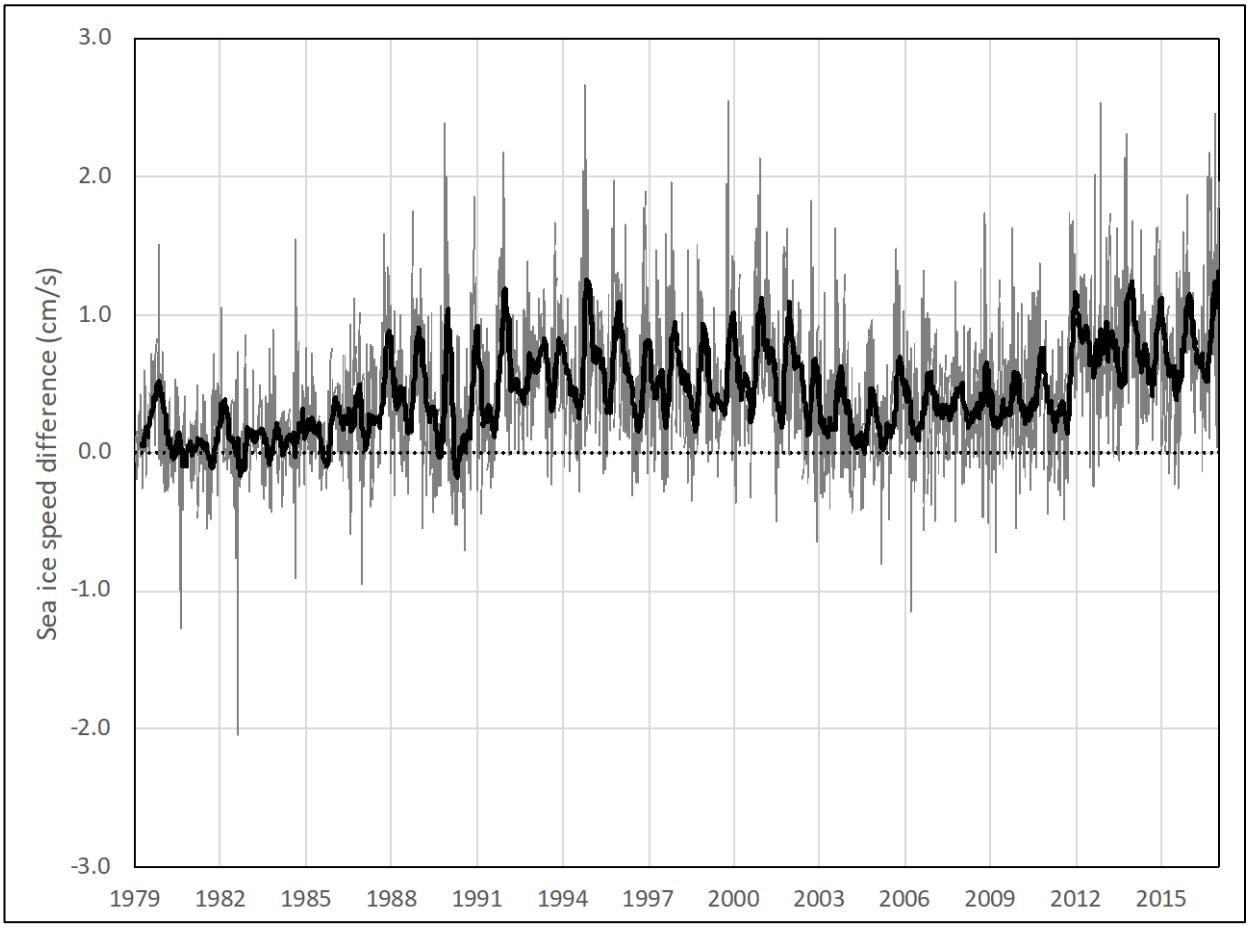

Figure 7. Arctic weekly average sea ice drift speed difference between Version 4 and Version 3 (V4-V3), 1979-2017. A 13-week running average is overlaid on the weekly values to highlight seasonal variability.

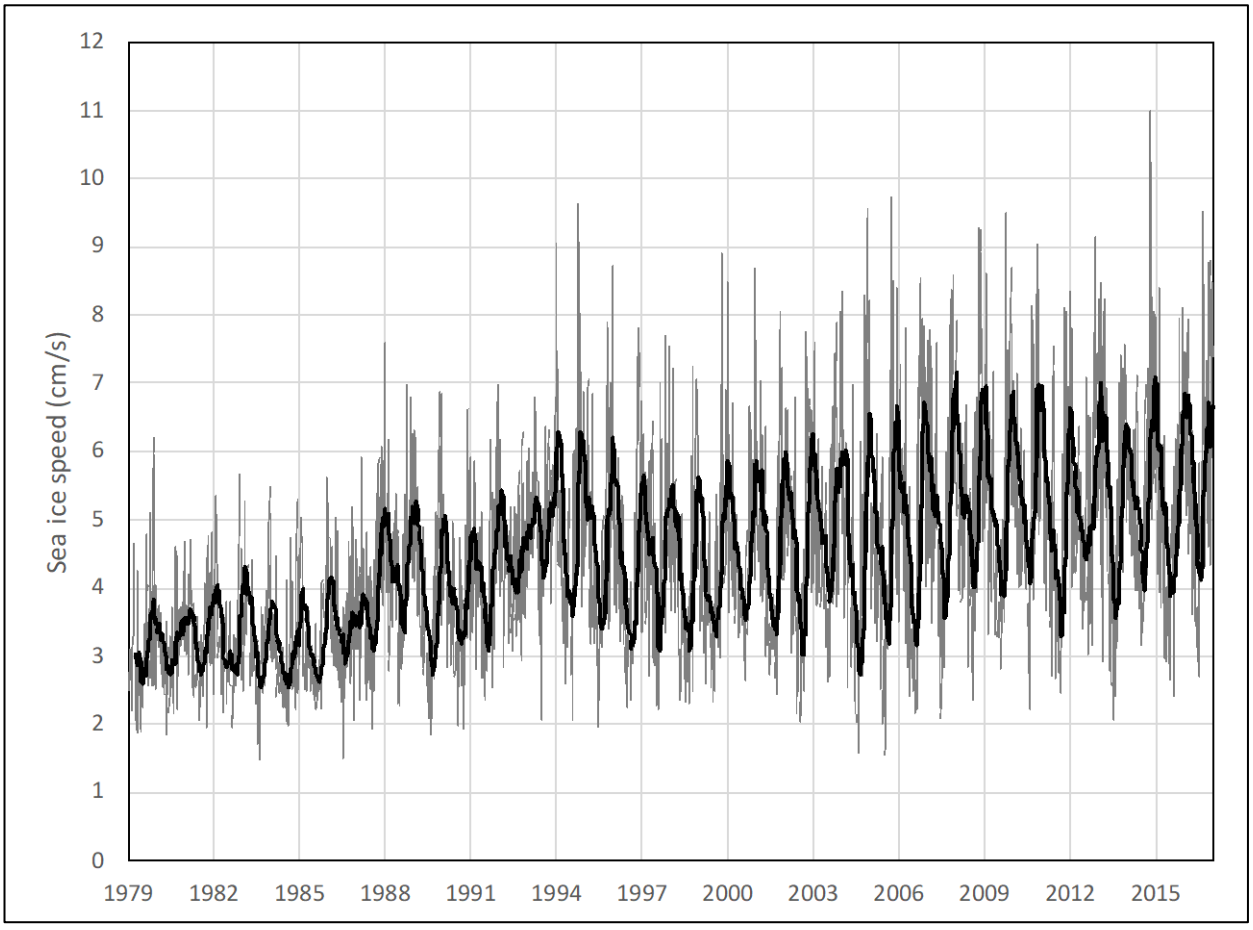

Figure 8. Arctic weekly average sea ice drift speed for Version 4, 1979-2017. A 13-week running average is overlaid on the weekly values to highlight seasonal variability.

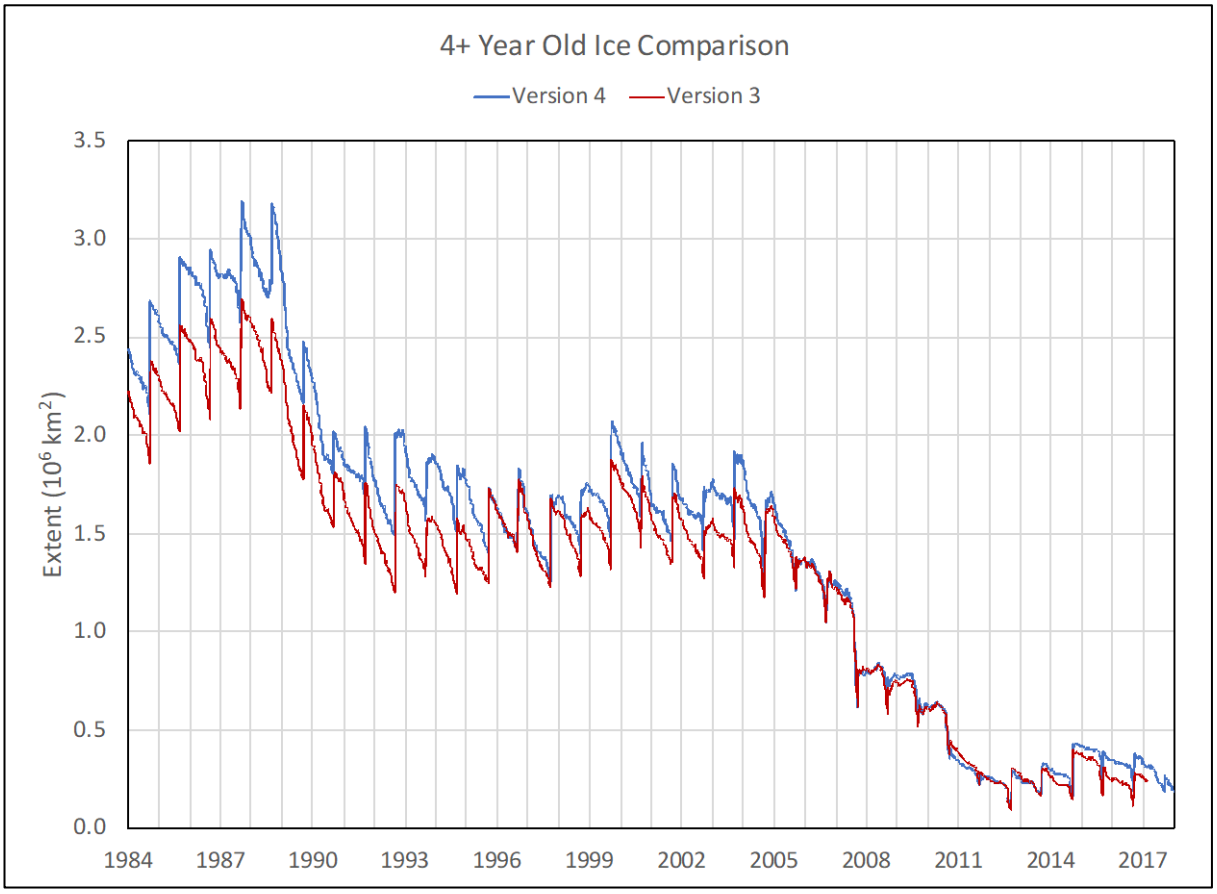

Figure 9. Comparison of 4+ year old ice from Version 3 (red) and Version 4 (blue) for 1984-2017.

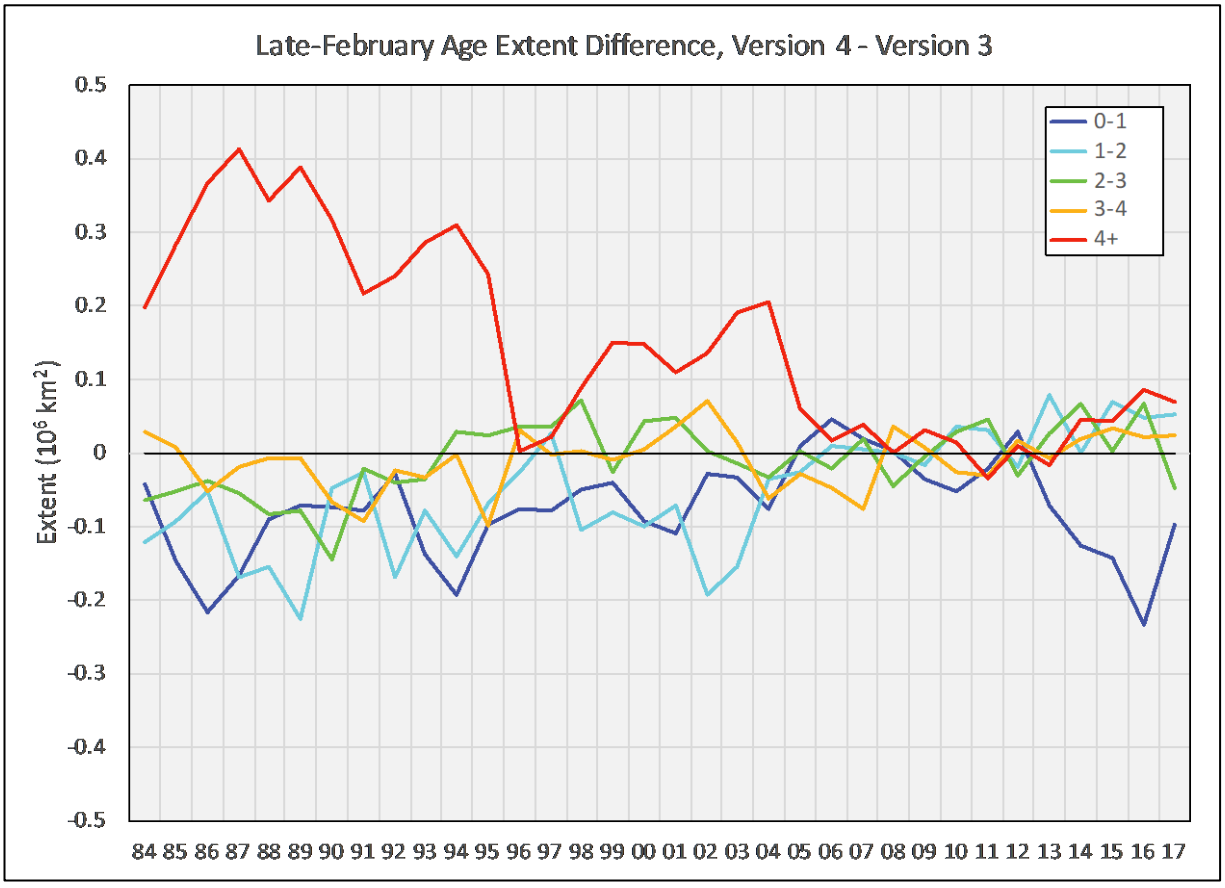

Figure 10. Extent difference between Version 4 and Version 3 sea ice age categories for the week of February 19-25 from 1984 to 2017.

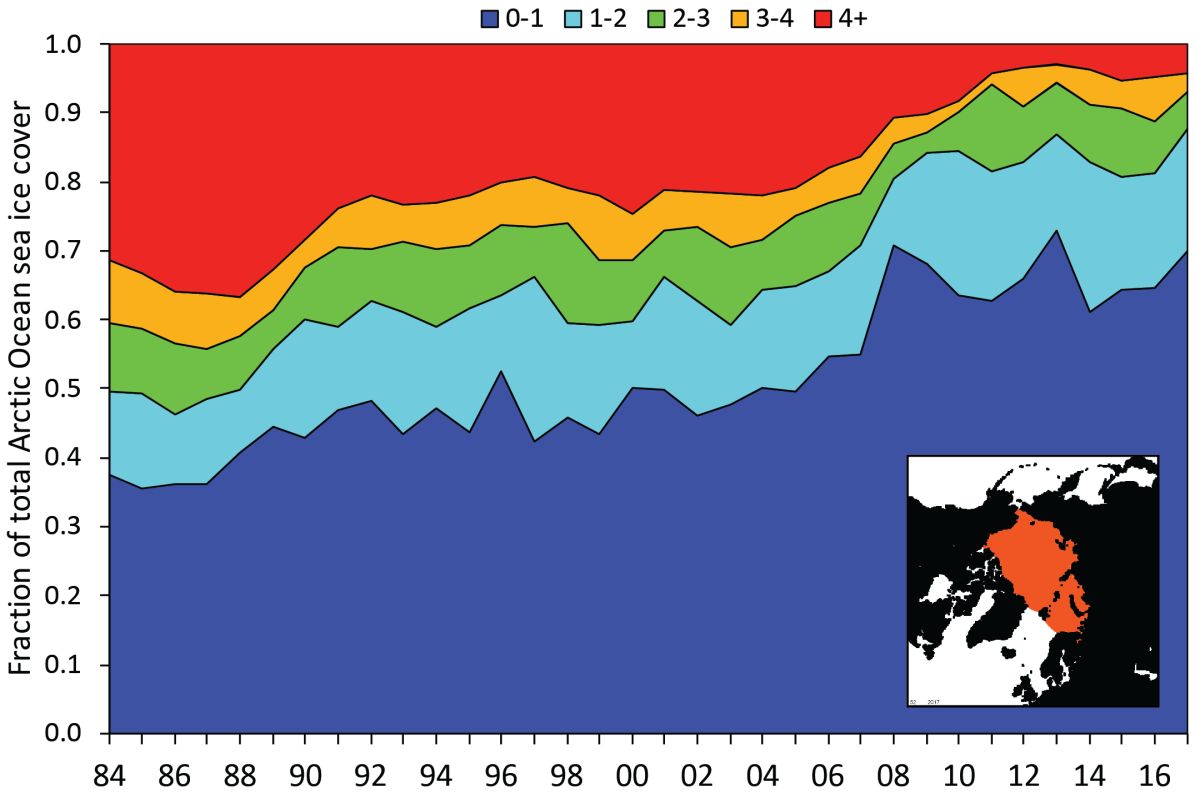

Figure 11. Trends in fraction of total sea ice coverage by sea ice age category for the week of February 19-25, 1984-2017. These trends are for the Arctic Ocean region, which is the region shaded in orange in the lower right inset image.